Journal of Orthopaedic Translation 30 (2021) 6–15

Contents lists available at ScienceDirect

Journal of Orthopaedic Translation

journal homepage: www.journals.elsevier.com/journal-of-orthopaedic-translation

Dual-functional hybrid quaternized chitosan/Mg/alginate dressing with antibacterial and angiogenic potential for diabetic wound healing

Minqi Wang, Yiqi Yang, Kai Yuan, Shengbing Yang **, Tingting Tang *

Shanghai Key Laboratory of Orthopaedic Implants, Department of Orthopaedic Surgery, Shanghai Ninth People's Hospital, Shanghai Jiao Tong University School of Medicine, Shanghai, China

ARTICLE INFO

Keywords:
Functional dressing
Quaternized chitosan
Magnesium
Diabetic wound

ABSTRACT

Background: Clinic treatment of diabetic foot ulcers (DFUs) is considerably challenging. Impaired wound healing may be caused by poor vascularization and dysfunction of the extracellular matrix, which leads to poor re-epithelialization and increased risk of infection. In this study, we evaluated the treatment potential of a functional dressing comprising quaternized chitosan (hydroxypropyltrimethyl ammonium chloride chitosan) and magnesium (Mg) on DFUs.

Methods: Dressings were prepared by vacuum freeze-drying. The cellular proliferation, migration, and angiogenesis potential of the functional dressings were determined in vitro. Methicillin-resistant *Staphylococcus aureus* (MRSA, ATCC43300) and methicillin-resistant *Staphylococcus epidermidis* 287 (MRSE287) were used to evaluate the antibacterial efficiency of the dressings. Finally, a diabetic rat model with infected wounds was used to further evaluate the effects of functional dressings on the healing of DFUs.

Results: Functional dressings facilitated the migration of human dermal fibroblasts and human umbilical vein endothelial cells (HUVECs), while also stimulating angiogenesis in HUVECs. Additionally, the functional dressing could effectively eradicate MRSA and MRSE, exhibiting excellent antibacterial ability against drug-resistant bacteria. The results of in vivo microbiological and histological tests demonstrated effective anti-infection ability and wound-healing potential of this functional dressing.

Conclusions: The dual-functional dressing exhibited wound-healing ability and anti-infection efficiency, demonstrating potential application prospects in DFU treatment.

Translational potential of this article: As one of the common and serious complications of diabetes, DFUs do not heal easily, causing great suffering to patients. Therefore, improvement in the prognosis of DFUs is a crucial clinical need. The dual-functional dressing prepared in this study was proven to improve the treatment of DFUs, both in vitro and in vivo. Considering its urgent clinical necessity and good biocompatibility of its raw materials, such as alginate, Mg, and chitosan derivatives, this dual-functional dressing presents good prospects for clinical translation.

1. Introduction

Diabetes is a prevalent chronic disease with serious complications that disrupt the normal life of patients. It has been reported that there are an estimated 285 million patients with diabetes worldwide, which is expected to increase to 439 million by 2030. In North America and Europe, the number of adults with diabetes is expected to increase by 42.4 % and 20 %, respectively, and a major surge in Africa is predicted, with the number of adults with diabetes expected to increase by 98.1 % from 2010 to 2030 [1,2]. As the most common complication of diabetes, the incidence of diabetic foot ulcers (DFUs) is 15 % [3]. Furthermore, with the development of DFUs, patients have presented with osteomyelitis and eventually undergone amputation [4,5]. Moreover, with DFUs, there is a high risk of infection due to the damaged local vessels and migration of immune cells; further, the local antibiotic accumulation could be poorly confined, which can compromise the second defense line.

* Corresponding author. Shanghai Key Laboratory of Orthopedic Implants, Department of Orthopedic Surgery, Shanghai Ninth People's Hospital, Shanghai Jiao Tong University School of Medicine, Zhizaoju Road 639, Shanghai, 200011, China.

** Corresponding author. Shanghai Key Laboratory of Orthopedic Implants, Department of Orthopedic Surgery, Shanghai Ninth People's Hospital, Shanghai Jiao Tong University School of Medicine, Zhizaoju Road 639, Shanghai, 200011, China.

E-mail addresses: bioshengbingy@163.com (S. Yang), ttt@sjtu.edu.cn (T. Tang).

https://doi.org/10.1016/j.jot.2021.07.006
Received 20 April 2021; Received in revised form 25 July 2021; Accepted 27 July 2021

The development of local infection causes secondary damage to the tissues within the wound by continuous over-activated inflammation, direct toxicity of bacteria, and formation of abscesses or necrotic tissues. Once the DFUs are infected, the difficulty in wound healing will further increase [6].

Clinically, debridement and systemic and local antibiotic management are commonly adopted to treat DFUs, although the prognosis is not satisfactory [7]. In addition, clinical researchers have recently explored the efficiency of certain new therapies for DFUs, such as punch grafting, negative pressure wound therapy, and magnetic fields [8–10]. In addition, considerable research has been conducted for promoting wound healing, among which the local application of growth factors, such as β-fibroblast growth factor (β-FGF), epidermal growth factor (EGF), and vascular endothelial growth factor (VEGF), can significantly accelerate wound healing [11–15]. However, there also exist certain challenges that limit the local application of growth factors in chronic wounds, such as high dose requirements, protein instability and its short lifetime in vivo, and high cost [16]. Considering the disadvantages of the local usage of growth factors, studies on the wound-healing effects of bioactive metal ions are an alternative focus in this field [17]. It has been reported that magnesium ions (Mg) are associated with a variety of cell functions related to wound healing [18–20], including enhanced proliferation of keratinocytes [21], increased collagen production, and stability of fibroblast cells [22,23]. In addition, Mg can stimulate the proliferation and migration of human umbilical vein endothelial cells (HUVECs) [19] and regulate the expression of angiogenesis-related genes (HIF-1α and VEGF) [24]. We hypothesized that Mg may play an important role in diabetic wound healing by restoring decreased cellular migration and hindering local vascularization.

Many studies have been conducted on the prevention of wound infections, including dressings that contain antibiotics or certain antibacterial metals [25–27]. However, the prevalence of antibiotic-resistant bacteria and the possible toxicity of metal nanoparticles are the main disadvantages of these two types of anti-infection dressings [28,29]. In our previous studies, we synthesized a water-soluble chitosan derivative, hydroxypropyltrimethyl ammonium chloride chitosan (HACC). Interestingly, the antibacterial properties and biocompatibility of this derivative are related to the degree of substitution of its quaternary ammonium group, and we found an appropriate degree, at which HACC shows both good biocompatibility and excellent anti-infection ability [30]. We have constructed a variety of biomaterials loaded with HACC and confirmed that HACC has great potential to be loaded within tissue-repairing biomaterials [31,32].

In general, the treatment of diabetic chronic wounds faces certain challenges: 1) disturbed wound-healing steps and 2) high infection rate. In this study, we aimed to produce a dual-functional alginate dressing containing Mg and HACC. We hope that the functional dressing can promote wound healing and prevent the occurrence of infection, thus helping to treat unhealed diabetic ulcers.

2. Experimental section

2.1. Materials

Sodium alginate (viscosity = 200 ± 20 MPa), anhydrous calcium chloride, and magnesium chloride hexahydrate were purchased from the Aladdin Industrial Corporation (Shanghai, China). According to our previous study, HACC with a 26 % DS of quaternary ammonium was produced by combining chitosan and glycidyl trimethylammonium chloride (GTMAC) [32]. Chitosan (molecular weight = 5.0×10^4 g/mol, 87 % N-deacetylation) was purchased from Zhejiang Yuhuan Ocean Biochemistry Co., Ltd., China. N-Hydroxysuccinimide (NHS), 1-(3-dimethylaminopropyl)-3-ethylcarbodiimide hydrochloride (EDC.HCl), 1, 4-dioxane, and GTMAC were purchased from Sigma–Aldrich, USA. Human dermal fibroblasts (HDFs; PCS-201-012) and HUVEC (PCS-100-010) were obtained from the American Type Culture Collection (ATCC), while human keratinocyte cells (HaCaT) (ACC-771) cells was obtained from Deutsche Sammlung von Mikroorganismen und Zellkulturen (DSMZ).

2.2. Preparation of alginate dressing

The vacuum freeze-drying method was employed to prepare the alginate dressing. Briefly, 2 % sodium alginate was dissolved in deionized water and fully blended overnight to form a homogeneous solution. One milliliter of alginate solution was pipetted into each well of a tissue culture plate (basal area = 2 cm^2), followed by freeze-drying for 24 h. Calcium chloride (5 %) was used in the cross-linking procedure and the dressing was then freeze-dried again for another 24 h. The obtained calcium alginate films were then soaked in 1 mg/ml HACC and 100 mM magnesium chloride solution for 2 h. In total, we obtained three groups of dressings: Ctrl, HACC, and HACC + Mg. The membranes were then freeze-dried for a third time.

2.3. Morphological characterization

The surface morphologies of the dressings were observed by scanning electron microscopy (SEM, S-4800, Hitachi Ltd., Tokyo, Japan) operated at 5 kV. Samples were sprayed with a layer of gold-palladium before observation. Randomly selected fields on each sample were scanned at both low and high magnifications.

2.4. Swelling property

The swelling rate of the dressing was determined by soaking the films in phosphate-buffered saline (PBS) at 37 °C. At predetermined time points (5, 10, 15, 30, 45, and 60 min), the films were taken from PBS and immediately weighed after removing the excess fluid remaining on the surface. The swelling rate of the dressings was calculated by the swelling ratio = (Ws − Wd)/Wd, where Wd is the weight of the dried dressing and Ws is the weight of the swollen dressing.

2.5. Release in vitro

An in vitro release test was carried out by incubating the dressings (basal area = 2 cm^2) in PBS solution (pH = 7.4) at a mass volume ratio of 1 g:15 ml at 37 °C under agitation at 100 rpm. At predetermined time points, the concentration of the release media was measured using inductively coupled plasma mass spectrometry (ICP, Agilent 710, California, USA).

2.6. Cell viability

HaCaT cells and HDFs were used in this study. These cells were cultured in Dulbecco's modified Eagle's medium (DMEM, Hyclone, USA) supplemented with 10 % fetal bovine serum (FBS, Gibco, USA), 100 U ml^{-1} of penicillin (Hyclone), and 100 μg/ml of streptomycin (Hyclone) at 37 °C in a humidified atmosphere with 5 % CO_2. Both dressings used for the in vitro and in vivo parts were sterilized by UV exposure for 30 min on each side, and all operations were strictly aseptic. In this section, dressing extractions were prepared using a cell culture medium. The sterilized dressings (basal area = 2 cm^2) were incubated in DMEM at a mass volume ratio of 1 g:15 ml [33]. After agitation at 100 rpm for 24 h, the supernatant was carefully pipetted into a new sterile tube and stored at 4 °C until further use.

2.6.1. Cell adhesion test

Cells were cultured with sterilized dressings at a density of approximately 1×10^5 cells/ml for 24 h. The cells were then stained with LiveDead Viability dye (L3224; Thermo Fisher Scientific, USA) for 15 min. After discarding excess dye and washing three times with PBS, confocal laser scanning microscopy (CLSM, TCS SP8, Leica Microsystems,

Germany) was used to visualize cell adhesion on the dressings. Green fluorescence represents living cells, with an excitation wavelength of 490 nm and an emission wavelength of 515 nm. Meanwhile, red fluorescence indicates dead cells, with an excitation wavelength of 535 nm and an emission wavelength of 617 nm.

2.6.2. CCK8 assay

Two-hundred microliters of cell suspension at a density of 1×10^5 cells/ml were seeded in each well of a 96 well plate. After overnight culture, different dressing groups were added. The biocompatibility of the materials was estimated using the CCK8 kit (DOJINDO, Japan) at time points of 24, 48, and 72 h. The modified optical density (OD) values at 48 and 72 h were normalized to those at 24 h to calculate the cell proliferation rate. The reagent was diluted 10 times with DMEM containing 10 % FBS and incubated with cells at 37 °C for 2 h. The OD at 450 nm was measured using an enzyme-linked immunosorbent assay reader (Thermo Varioskan Flash, USA).

2.7. Scratch wound assay

The influence of dressings on the migration of HUVECs and HDFs was assessed in vitro using a scratch wound assay. Briefly, cells were seeded into 24 well plates at a density of 1×10^5 cells/well. Once confluent, the cells were starved overnight with 1 % FBS medium to minimize the interference of cell proliferation. A straight line at the medium of the cell monolayer was created using a 200 μL pipette tip. Cell debris was gently removed by PBS. Different groups of dressing extractions were then added into each well and incubated at 37 °C for 24 h.

2.8. In vitro sprouting analysis

Fifty microliters of growth factor-reduced Matrigel (BD Biosciences, USA) was pipetted into each well of a 96-well plate on ice, and then incubated in an incubator at 37 °C for 30 min to allow gelation. The pretreated HUVECs with different dressing extracts were seeded on the surface of the gel at a density of 1×10^5 cells/well. After 6 h of incubation at 37 °C, the cells were fixed with 2.5 % glutaraldehyde and then stained with calcein. The capillary tube length and number of branch points were quantified.

2.9. Antimicrobial activity

Methicillin-resistant *Staphylococcus aureus* (MRSA, ATCC43300) and methicillin-resistant *Staphylococcus epidermidis* 287 (MRSE287) were selected to study the antibacterial efficiency of the dressings in vitro. The former was purchased from the American Type Culture Collection (Manassas, VA, USA) and the latter was isolated from an infected patient at Shanghai Ninth People's Hospital (Shanghai, China). The above-mentioned bacteria were both cultured in tryptic soy broth (TSB).

2.9.1. Spread plate method

The number of bacteria adhering to the dressings was counted using the spread plate method. After overnight proliferation, the concentration of the bacterial suspension was adjusted to 10^6 CFU/ml. Both groups of dressings were incubated with bacteria for 24 h at 37 °C. The dressings were gently washed with PBS three times and placed in sterile centrifuge tubes containing 2 ml PBS. An ultrasonic bath (50 Hz, 10 min) was used to release the bacteria that firmly adhered to the surface of the dressings. The suspension was serially diluted and seeded onto tryptic soy agar (TSA). After incubation at 37 °C for 24 h, the plates were photographed and the bacterial colonies on the TSA were counted.

2.9.2. Live/dead bacterial assay

The materials were incubated with MRSA for 24 h, as described above. After gently rinsing three times in PBS, the dressings were stained with 1 ml of combined dye (LIVE/DEAD Baclight viability kits, L7012; Thermo Fisher Scientific, USA) in the dark for 15 min. The dressings were then washed with PBS three times before CLSM detection.

2.9.3. Transmission electron microscopy

First, the three dressing groups were prepared by incubating the dressings (basal area = 2 cm^2) in TSB according to the protocol described in Section 2.6. The bacterial suspension at a concentration of 1×10^7 CFU/ml was cultured with prepared dressing extractions for 1 h at 37 °C and then harvested by centrifugation at 5000×*g* for 5 min. The bacteria were washed twice using PBS and fixed with 2.5 % glutaraldehyde for 2 h. Transmission electron microscopy (TEM, Tecnai G20, FEI, USA) was used to image the bacteria morphology.

2.10. In vivo evaluation of wound-healing efficiency of functional dressing on DFUs

All animal experiments were approved by the Animal Ethics Committee of the Shanghai Ninth People's Hospital. Eight-week-old female Sprague Dawley (SD) rats were induced to diabetes by a single intraperitoneal injection of streptozotocin at 90 mg/kg body weight dissolved in sodium citrate buffer (0.1 M, pH 4.5). The glucose level of the rats was monitored twice a week and above 300 mg/dl indicated successful building of the diabetic model [34]. When the glucose level was below 300 mg/dl, streptozotocin injection was repeated. Rats with stable high blood glucose levels for two weeks were used in subsequent wound-healing experiments.

2.10.1. Wound healing

Diabetic rats were randomly divided into three groups and anesthetized by intraperitoneal injection of pentobarbital sodium (50 mg/kg). After shaving the dorsal hair and sterilizing the skin, two full-thickness skin defects, with a diameter of 10 mm, were created with scissors on the back of each rat. A bioluminescent *S. aureus* strain (Xen29) suspension at a concentration of 10^8 CFU/ml was prepared, and 50 μl of this suspension was added to each wound. Then, the wounds were covered with different dressings, including blank alginate dressing, dressing containing only HACC, and dressing loaded with both HACC and Mg. The dressings were changed every two days. Photographs of the wounds were taken at predetermined time points (0, 2nd, 4th, 7th, 10th, and 14th days post-surgery) and Image J (1.52q, National Institutes of Health, USA) was used to measure the wound area. The healing rate was then calculated.

2.10.2. Real-time monitoring of wound infection

As Xen29 was used, wound infection severity can be reflected by the intensity of the bioluminescent signal. Therefore, to compare the infection development among different groups, diabetic rats with infected wounds were detected on days 2 and 4 after surgery using an IVIS Spectrum® imaging system (Caliper, PerkinElmer Company, USA). In vivo bioluminescent signals were quantified in terms of the average radiance (p/s/cm^2/sr) within a region of interest (ROI, n = 4).

2.10.3. Microbiological evaluation

Tissue around the wound was collected from the enthanized rats on day 14 and then placed in a sterile tube. After freezing in liquid nitrogen for 10 min, the samples were fully ground. Subsequently, the ground tissue was resuspended in 2 ml PBS, and the spread plate method was used to compare the number of bacteria between different groups (n = 4).

2.10.4. Histopathological evaluation

After euthanizing the rat on the 14th day, samples containing wound and adjacent normal tissues were collected and fixed with 4 % paraformaldehyde for 48 h. After embedding in paraffin, the samples were sectioned at 5 μm intervals. Hematoxylin and eosin (H&E) and Masson's trichrome staining were used to assess re-epithelialization and collagen deposition in the wound.

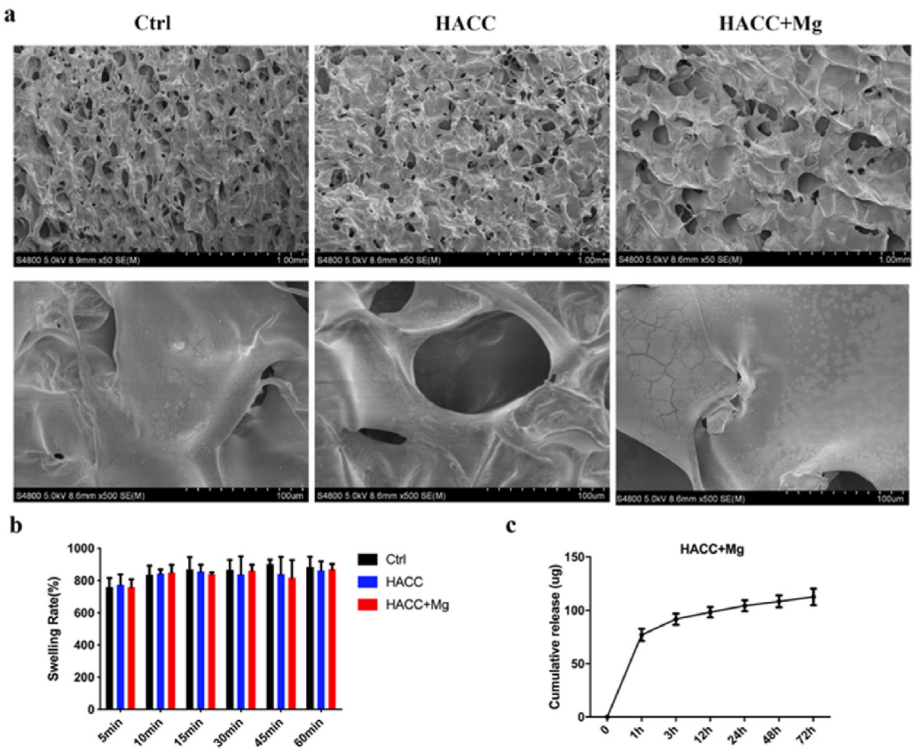

Fig. 1. Characterization of functional dressing. (a) SEM images of three group dressings. (b) Swelling rate of dressings. (c) Cumulative release curve of magnesium.

2.11. Statistical analysis

All quantitative data are expressed as the mean ± standard error. In vitro experiments were performed in triplicate. Statistical analysis was performed using analysis of variance (ANOVA). The threshold for statistically significant differences was $p < 0.05$.

3. Results

3.1. Characterization of functional dressings

SEM was used to observe the surface morphology of the dressings. As shown in Fig. 1a, both the blank alginate dressing and the functional

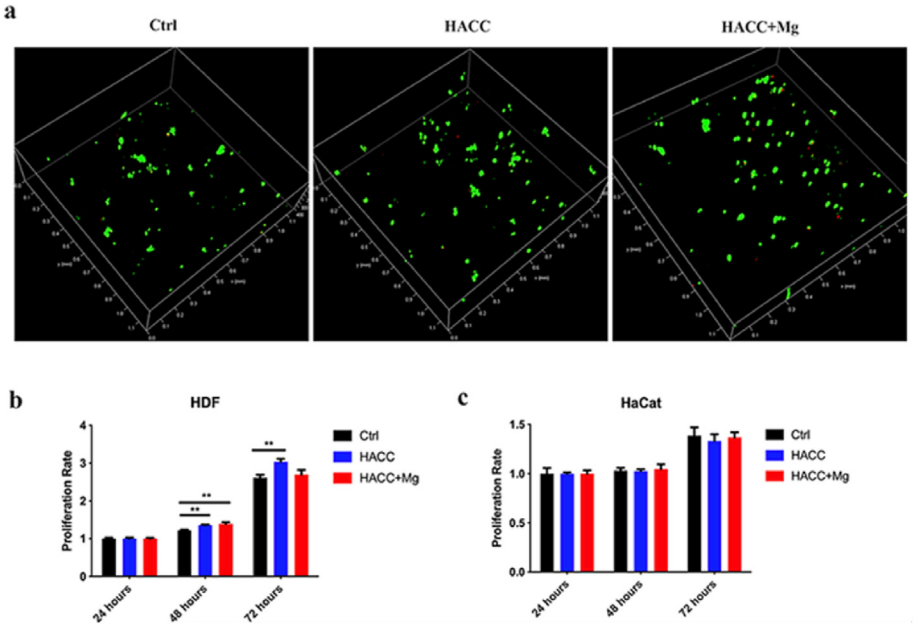

Fig. 2. Biocompatibility of functional dressing. (a) CLSM images of HDF attachment. (b) CCK8 results of HDF proliferation. (c) CCK8 results of HaCat proliferation. ** indicates $p < 0.01$.

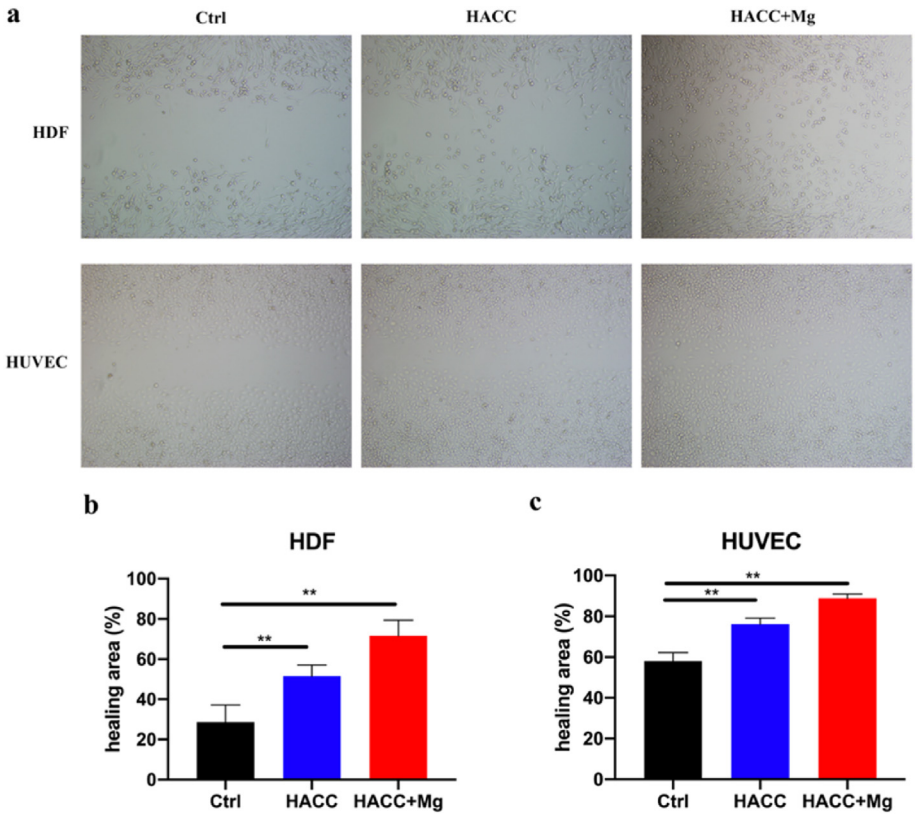

Fig. 3. Results of cell migration assay in vitro. (a) Images of HDF and HUVEC cells migration after cultured for 24 h. (b) and (c) quantitatively calculate the percentage of healing area. ** indicates $p < 0.01$.

dressing showed a porous structure, indicating that the loading of active elements and subsequent freeze-drying processes do not significantly influence the porous structure of the dressings. Considering that the porous structure of a dressing may impact its wound-healing efficacy, keeping the porous structure similar among different groups is helpful to eliminate the potential influence of morphological factors.

The swelling ratio reflects the water absorption capacity of the functional dressing, as shown in Fig. 1b. The three groups of dressings all showed good swelling properties and could absorb water of approximately eight times their initial weight in a short period of time. There was

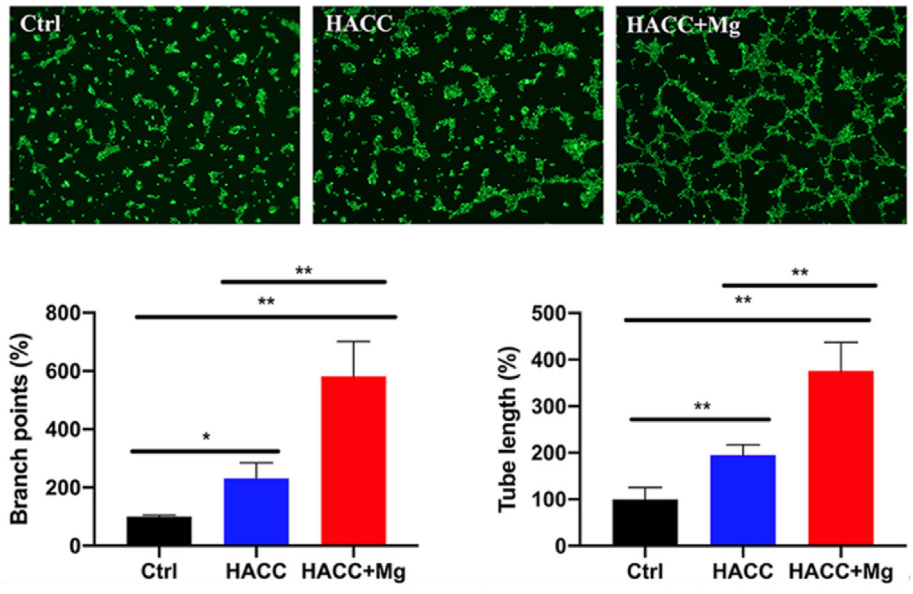

Fig. 4. Results of HUVEC sprouting analysis. * indicates $p < 0.05$ while ** indicates $p < 0.01$.

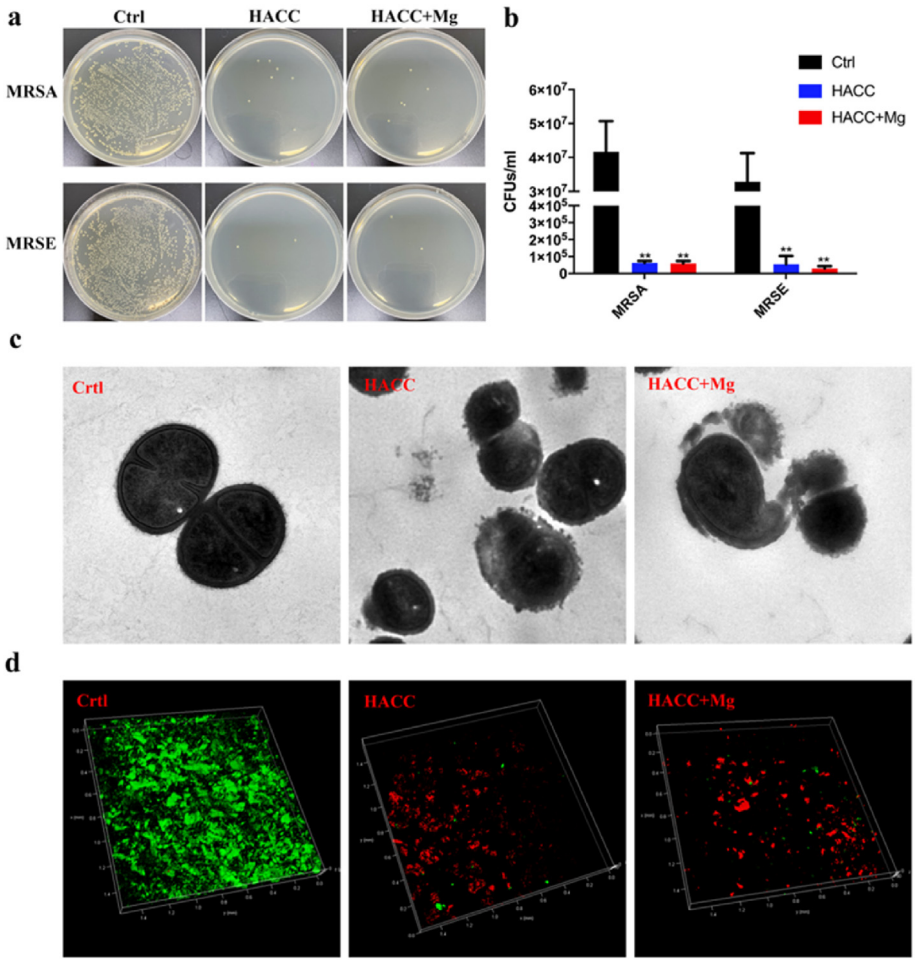

Fig. 5. Antibacterial results of the functional dressing in vitro. (a) images of bacterial clone on agar plates. (b) quantitative counting of bacteria on each group of dressings. (c) TEM images of MRSA after culturing with dressings. (4) CLSM images of bacteria on dressings, indicating biofilm formation and bacterial eradication. ** indicates $p < 0.01$ compared with control group.

no significant difference between the groups ($p > 0.05$).

The ICP results of the released Mg are shown in Fig. 1c. Magnesium ions were rapidly released in the first hour in the Mg + HACC group, and then the release slowed down.

3.2. Biocompatibility of functional dressings

LiveDead staining and CCK8 tests were used to evaluate the adhesion and proliferation of HaCaT and HDF cells on dressings. In Fig. 2a, CLSM images show that after 24 h of cultivation, the cells on the three dressing groups mainly emitted green fluorescence, indicating the viability of adhered cells. Then, the CCK8 test quantitatively analyzed the proliferation rate of cells on each dressing group. Fig. 2b and c shows that HDF proliferation was significantly improved by the HACC and HACC + Mg dressings ($p < 0.01$). However, there was no significant difference in HaCaT proliferation among the three dressing groups ($p > 0.05$). These results verified the good biocompatibility of the functional dressings.

3.3. In vitro cell migration assays

Fibroblasts can play an important role in the wound-healing process; for example, they migrate to the injured area and produce collagen, which is closely related to extracellular matrix (ECM) remodeling. In addition, HUVECs are another important cell involved in wound healing, mainly related to local vascularization. Therefore, the influence of the functional dressings on the migration of these two cells was tested. The healing area of HDF cells in the control group was 28.637 % ± 8.473 % of the scratch, while which of HUVECs was 58.007 % ± 4.216 %. Both the other two functional dressings significantly increased the migration ability of HDFs and HUVECs (Fig. 3).

3.4. In vitro sprouting analysis

The sprouting analysis of HUVECs can reflect the potency of dressings in promoting vascularization. Compared with the control group, HACC dressing promoted the sprouting of HUVECs to some extent. The dual-function dressing containing both HACC and Mg further promoted vascularization of HUVECs.

3.5. Antibacterial ability of functional dressing

Wound infection is another important obstacle that seriously hinders the healing of DFUs. The evaluation results of the antibacterial properties of the functional dressings are presented in this part.

3.5.1. Spread plate method

Both groups of HACC-containing dressings could effectively eradicate the bacteria attached to them. The bacterial counting results of MRSA and MRSE on HACC dressings were 6.33×10^4 and 5.5×10^4 CFU/ml, respectively, whereas they were 6.0×10^4 and 3.0×10^4 CFU/ml on the HACC + Mg group, respectively. However, many bacteria adhered to the control group dressing, which showed a significant difference compared

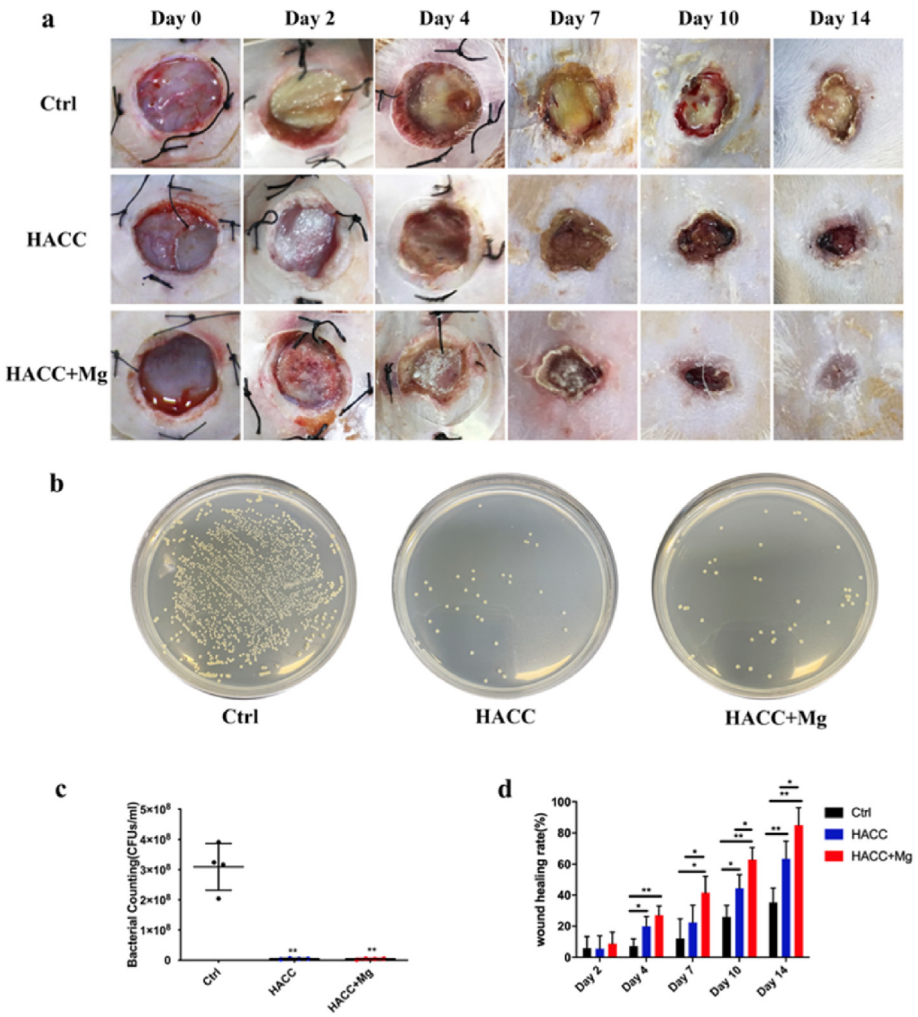

Fig. 6. Results of wound healing rate and microbiology assay. (a) Representative pictures of wound at pre-determined time points. (b) and (c) Counting of bacteria existed within wound tissue. (d) wound healing rate. * indicates $p < 0.05$ while ** indicates $p < 0.01$.

with the HACC-containing groups ($p < 0.01$). The above quantitative results of bacterial counting demonstrated efficient anti-infection ability of the dual-functional dressing, which could effectively eliminate antibiotic-resistant bacteria (Fig. 5a and b).

3.5.2. *Live/dead bacterial assay*

After LiveDead Bac staining, bacteria on the dressings were observed directly using CLSM. Fig. 5d shows that a large amount of biofilm formed on the dressing of the control group, which mainly express green fluorescence. On the dressings of the HACC and HACC + Mg groups, only a few green fluorescence (representing living bacteria) and some dead bacteria expressing red fluorescence were observed.

3.5.3. *TEM*

TEM was used to observe the morphology of MRSA. As shown in Fig. 5c, the bacteria in the control group were round in shape, and their walls were intact and smooth. After culturing with dressings of the HACC and HACC + Mg groups, the bacterial morphology became irregular and some bacteria were even broken. Therefore, destroying bacterial integrity can be considered a possible bactericidal mechanism of dressings containing HACC.

3.6. *In vivo wound-healing effect of functional dressing*

To further verify the efficiency of dual-functional dressings on wound healing, DFUs infected on the back of diabetic rats were selected. There were three groups: 1) control, calcium alginate dressing; 2) HACC, dressing containing only HACC; and 3) HACC + Mg, dual-functional dressings containing both Mg and HACC.

3.6.1. *Wound closure assay*

Images of the wound were taken at predetermined time points, and the wound area was measured using Image J. As shown in Fig. 6a and d, compared with the control group, both the HACC and HACC + Mg groups significantly promoted wound healing. In addition, wounds in the HACC + Mg group healed faster than those in the HACC group. At day 14, the wound-healing rates of control, HACC, and HACC + Mg groups were 35.32 ± 9.24 %, 63.49 ± 11.29 %, and 85.04 ± 11.25 % respectively. Wound areas in the control group were still large, and some yellow exudate was also present in the wound, which is considered an indication of wound infection (Fig. 6a and d).

3.6.2. *Microbiology assay of wounds*

The number of bacteria within the wound tissue was quantitatively evaluated. In the control group, a large number of bacteria existed in the tissue near the wounds, whereas the number of bacteria in the HACC and HACC + Mg groups decreased significantly. Thus, the HACC-loaded dressing effectively prevented wound infection in diabetic rats (Fig. 6b and c).

In addition, bioluminescent Xen29 was used to dynamically observe local infection development. On the 2nd day after surgery, the wounds covered with control dressing showed intense signals. Although the

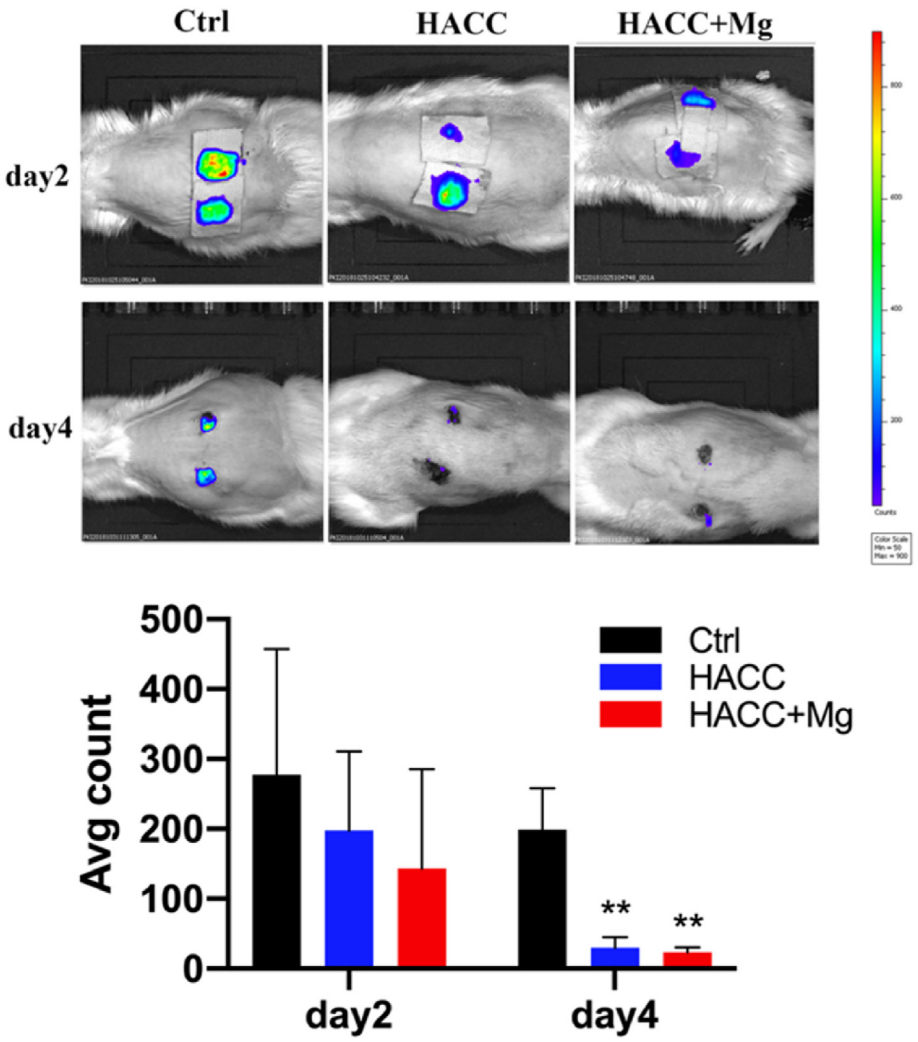

Fig. 7. Dynamic observation of the signal intensity of bioluminescent bacteria. (a) showed representative images of infected wounds and (b) quantitatively evaluated the signal within the region of wounds. ** indicates $p < 0.01$ compared with control group.

fluorescence signal of wounds treated with HACC and HACC + Mg dressings appeared much weaker, there was no significant difference when compared with that of the control group ($p > 0.05$). On the 4th day after surgery, the bacterial fluorescence intensity of the control group weakened to some extent but was still significantly higher than that of the two HACC-containing groups (Fig. 7). Relevant studies have also reported that the fluorescence intensity of Xen29 weakens during infection development, which is considered to be due to the formation of mature biofilm. Pathogens within biofilms downregulate their metabolism, thus decreasing fluorescence intensity.

3.6.3. *Histology analysis*

As shown in the H&E staining section, there were some necrotic tissues (indicated by black areas) in the control group, whereas fewer necrotic tissues were found in the other two groups. Moreover, the wound size in the control group was still large, whereas in the HACC + Mg group, it was almost healed. Masson staining indicates collagen deposition within the wound, in which collagen is stained blue. In the control group, although collagen deposition stained blue was observed, the structure was disordered. In the HACC + Mg group, compared with the other two groups, there was a deep blue-stained area, and the collagen structure was orderly, demonstrating better wound ECM repair.

4. Discussions

Aiming to help the treatment of chronic unhealing DFU wounds, we designed a dual-functional dressing in this study, which decreased the infection rate and improved the limited wound-healing process. Mg and HACC were selected as the main elements in the functional dressing. The results showed that the dual-functional dressing can promote the migration of fibroblasts and endothelial cells, stimulate local angiogenesis, effectively eradicate bacteria, and ultimately greatly improve the healing of DFUs.

In this study, both keratinocytes and fibroblasts were used to evaluate the biological activities of the functional dressings. Although no significant effect was observed on the proliferation of keratinocytes, the dressing promoted the proliferation of fibroblasts. We speculate that this difference may be caused by slower proliferation of keratinocytes. The OD value of keratinocytes tested during the CCK8 assay was significantly lower than that of fibroblasts at each time point. In addition, dressing can also greatly promote the migration of fibroblasts and vascular endothelial cells. Migration is the first step for fibroblasts to play the role of granulation tissue formation and collagen deposition. After stimulation with the HACC + Mg dressing, the migration rate of fibroblasts reached 57.8 ± 6.99 %, which was significantly higher than that of the control group. In addition, the migration of HUVECs was also greatly improved under the stimulation of the HACC + Mg dressing, which was considered closely related to neovascularization (Fig. 3). The in vitro sprouting assay

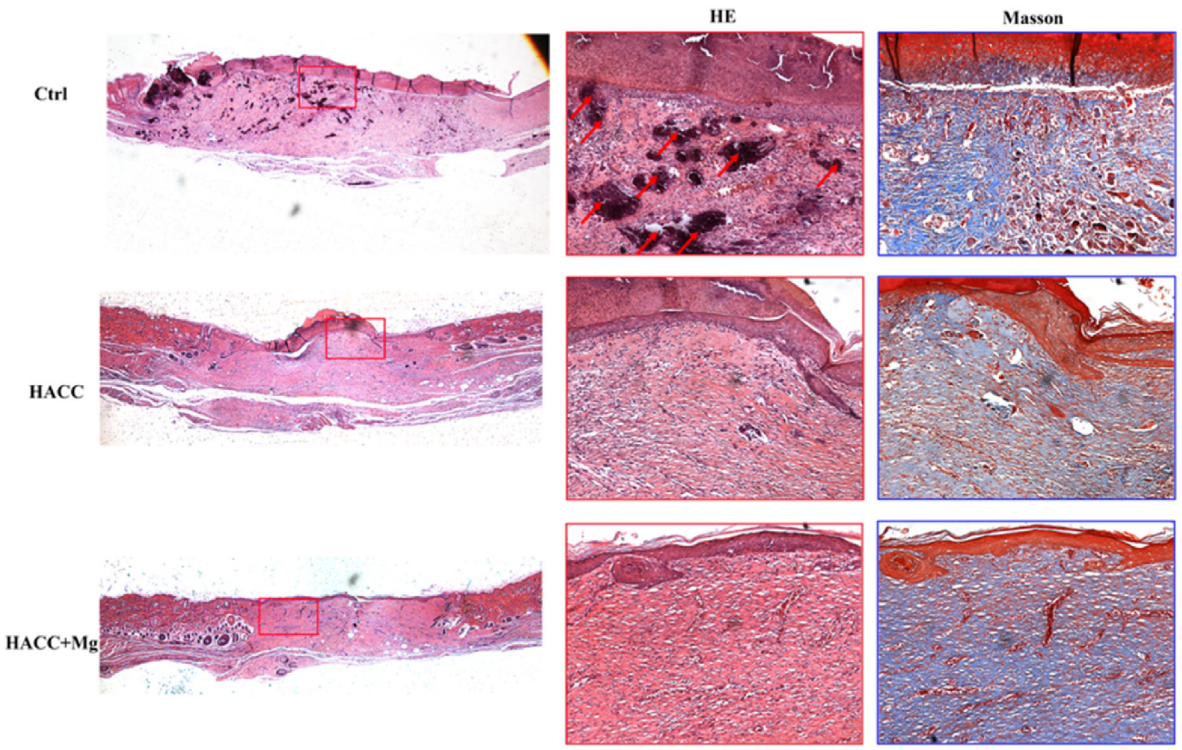

Fig. 8. HE staining and masson staining images of wound in different groups. The red boxes indicate enlarged view of HE staining while the blue boxes indicate enlarged view of masson staining. The red arrows indicated the necrotic tissue that shown as black area.

shown in Fig. 4 directly tested the ability of the dressing to promote angiogenesis. A quantitative analysis confirmed that the dual-functional dressing can greatly increase the number of newly formed vessels. Thus, dual-functional dressing is expected to salvage obstructed angiogenesis in diabetic wounds.

As mentioned in the introduction, excessively long wound exposure time, weakened immune defense, and the presence of drug-resistant bacteria all contribute to the development of DFU infection [35]. Drug-resistant bacterial strains, including MRSA and MRSE, were used to evaluate the antibacterial potential, and the results indicated that the addition of HACC significantly inhibited bacterial growth and biofilm formation. Furthermore, TEM images showed that the bacterial wall appeared abnormal or even ruptured after incubation with the two groups of HACC-containing dressings, which proves that the main antibacterial mechanism of HACC is to destroy the integrity of the bacterial outer membrane through physical interaction. However, as indicated in the supplementary information, the dressing containing Mg alone did not significantly inhibit bacterial growth, which seems not to be in accordance with previous findings [36]. We believe that this difference in the antibacterial properties of magnesium may be caused by different forms of raw material. Mg in the form of metal particles causes an alkaline microenvironment, which is considered the main reason for its antibacterial potential [37].

As shown in Figs. 7 and 8, the healing of infected wounds in rats of the control group was significantly restricted, which was also accompanied by yellow pus-like exudation. In addition, HE staining showed that necrotic tissue was present in the infected wounds. The anti-infection strategy for DFU treatment in this study can be divided into two parts. On the one hand, as a new chitosan derivative discovered in our previous research, HACC can effectively kill several kinds of bacteria under the appropriate degree of substitution, including antibiotic-resistant pathogens [30,31]. What's more, dual-functional dressing can accelerate wound healing, thus recovering the “first defense line” of the skin. Considering its urgent clinical necessity and the good biocompatibility of its raw materials, such as alginate, Mg, and chitosan derivatives, this dual-functional dressing showed good prospects for clinical translation.

5. Conclusion

In general, the dual-functional dressing proposed in this study can effectively accelerate DFU healing. On the one hand, the functional dressing showed good biocompatibility, promoted the migration of HDFs and HUVECs, and stimulated angiogenesis of HUVECs. In contrast, HACC is the main antibacterial element that can effectively eradicate antibiotic-resistant bacteria, including MRSA and MRSE. The excellent performance in the treatment of chronic unhealing wounds exhibited by the functional dressing demonstrates its great potential for clinical applications.

Funding

This work was supported by the Shanghai Science and Technology Development Fund (18441902700 and 18DZ2291200) and the National Natural Science Foundation of China (81802178).

Declaration of competing interest

The authors declare that they have no competing financial interests or personal relationships that could have appeared to influence the work reported in this paper.

Appendix A. Supplementary data

Supplementary data to this article can be found online at https://doi.org/10.1016/j.jot.2021.07.006.

References

[1] Shaw JE, Sicree RA, Zimmet PZ. Global estimates of the prevalence of diabetes for 2010 and 2030. Diabetes Res Clin Pract 2010;87(1):4–14.

[2] Whiting DR, Guariguata L, Weil C, Shaw J. IDF diabetes atlas: global estimates of the prevalence of diabetes for 2011 and 2030. Diabetes Res Clin Pract 2011;94(3):311–21.
[3] Tan CT, Liang K, Ngo ZH, Dube CT, Lim CY. *Application of 3D bioprinting technologies to the management and treatment of diabetic foot ulcers.* Biomedicines 2020;8(10).
[4] Lázaro-Martínez JL, García-Madrid M, García-Álvarez Y, Álvaro-Afonso FJ, Sanz-Corbalán I, García-Morales E. Conservative surgery for chronic diabetic foot osteomyelitis: procedures and recommendations. J Clin Orthop Trauma 2021;16:86–98.
[5] Ha Van G, Amouyal C, Bourron O, Aubert C, Carlier A, Mosbah H, et al. Diabetic foot ulcer management in a multidisciplinary foot centre: one-year healing, amputation and mortality rate. J Wound Care 2020;29(8):464–71.
[6] Pitocco D, Spanu T, Di Leo M, Vitiello R, Rizzi A, Tartaglione L, et al. Diabetic foot infections: a comprehensive overview. Eur Rev Med Pharmacol Sci 2019;23(2 Suppl):26–37.
[7] Boulton AJM, Armstrong DG, Hardman MJ, Malone M, Embil JM, Attinger CE, et al. Diagnosis and management of diabetic foot infections. American Diabetes Association 2020.
[8] Ji S, Liu X, Huang J, Bao J, Chen Z, Han C, et al. Consensus on the application of negative pressure wound therapy of diabetic foot wounds. Burns Trauma 2021:9. p. tkab018.
[9] Lv H, Liu J, Zhen C, Wang Y, Wei Y, Ren W, et al. Magnetic fields as a potential therapy for diabetic wounds based on animal experiments and clinical trials. Cell Prolif 2021;(3):54. p. e12982.
[10] García-Madrid M, Sanz-Corbalán I, Tardáguila-García A, Molines-Barroso RJ, López-Moral M, Lázaro-Martínez JL. Punch grafting for the management of hard-to-heal diabetic foot ulcers: a prospective case series. Int J Low Extrem Wounds 2021. 15347346211031085.
[11] Kim J, Lee KM, Han SH, Ko EA, Yoon DS, Park IK, et al. Development of stabilized dual growth factor-loaded hyaluronate collagen dressing matrix. J Tissue Eng 2021;12:1–13.
[12] Catanzano O, Quaglia F, Boateng JS. Wound dressings as growth factor delivery platforms for chronic wound healing. Expet Opin Drug Deliv 2021:1–23.
[13] Asiri A, Saidin S, Sani MH, Al-Ashwal RH. Epidermal and fibroblast growth factors incorporated polyvinyl alcohol electrospun nanofibers as biological dressing scaffold. Sci Rep 2021;11(1):5634.
[14] Hopkins C, Qin L. Innovative designs and procedures for fracture fixation and soft tissue repair. J Orthop Translat 2020;24:A1–a2.
[15] Dreyer CH, Kjaergaard K, Ding M, Qin L. Vascular endothelial growth factor for in vivo bone formation: a systematic review. J Orthop Translat 2020;24:46–57.
[16] Lo KW, Jiang T, Gagnon KA, Nelson C, Laurencin CT. Small-molecule based musculoskeletal regenerative engineering. Trends Biotechnol 2014;32(2):74–81.
[17] Zhang Z, Li W, Liu Y, Yang Z, Ma L, Zhuang H, et al. Design of a biofluid-absorbing bioactive sandwich-structured Zn-Si bioceramic composite wound dressing for hair follicle regeneration and skin burn wound healing. Bioact Mater 2021;6(7):1910–20.
[18] Sasaki Y, Sathi GA, Yamamoto O. Wound healing effect of bioactive ion released from Mg-smectite. Mater Sci Eng C Mater Biol Appl 2017;77:52–7.
[19] Banai S, Haggroth L, Epstein SE, Casscells W. Influence of extracellular magnesium on capillary endothelial cell proliferation and migration. Circ Res 1990;67(3):645–50.
[20] Lin X, Ge J, Wei D, Liu C, Tan L, Yang H, et al. *Surface degradation-enabled osseointegrative, angiogenic and antiinfective properties of magnesium-modified acrylic bone cement.* J Orthop Translat 2019;17:121–32.
[21] Tennenbaum T, Yuspa SH, Kapitulnik J. Magnesium and phosphate enrichment of culture medium stimulates the proliferation of epidermal cells from newborn and adult mice. J Cell Physiol 1990;143(3):431–8.
[22] Lin DJ, Hung FY, Yeh ML, Lui TS. Microstructure-modified biodegradable magnesium alloy for promoting cytocompatibility and wound healing in vitro. J Mater Sci Mater Med 2015;26(10):248.
[23] Lakra R, Kiran MS, Korrapati PS. Effect of magnesium ascorbyl phosphate on collagen stabilization for wound healing application. Int J Biol Macromol 2021;166:333–41.
[24] Gao P, Fan B, Yu X, Liu W, Wu J, Shi L, et al. Biofunctional magnesium coated Ti6Al4V scaffold enhances osteogenesis and angiogenesis in vitro and in vivo for orthopedic application. Bioact Mater 2020;5(3):680–93.
[25] Shi G, Wang Y, Derakhshanfar S, Xu K, Zhong W, Luo G, et al. Biomimicry of oil infused layer on 3D printed poly(dimethylsiloxane): non-fouling, antibacterial and promoting infected wound healing. Mater Sci Eng C Mater Biol Appl 2019;100:915–27.
[26] Singaravelu S, Ramanathan G, Sivagnanam UT. Dual-layered 3D nanofibrous matrix incorporated with dual drugs and their synergetic effect on accelerating wound healing through growth factor regulation. Mater Sci Eng C Mater Biol Appl 2017;76:37–49.
[27] Huang RK, Xie M, Zhao JJ, Xiao K, Kan WS. Posterior malleolar fracture: technique and clinical experience of the posterolateral approach. Chin J Traumatol 2012;15(1):23–6.
[28] Wahab MA, Li L, Li H, Abdala A. Silver nanoparticle-based nanocomposites for combating infectious pathogens: recent advances and future prospects. Nanomaterials 2021;11(3):581.
[29] Pang S, Gao Y, Wang F, Wang Y, Cao M, Zhang W, et al. Toxicity of silver nanoparticles on wound healing: a case study of zebrafish fin regeneration model. Sci Total Environ 2020;717:137178.
[30] Peng ZX, Wang L, Du L, Guo SR, Wang XQ, Tang TT. Adjustment of the antibacterial activity and biocompatibility of hydroxypropyltrimethyl ammonium chloride chitosan by varying the degree of substitution of quaternary ammonium. Carbohydr Polym 2010;81(2):275–83.
[31] Yang Y, Chu L, Yang S, Zhang H, Qin L, Guillaume O, et al. Dual-functional 3D-printed composite scaffold for inhibiting bacterial infection and promoting bone regeneration in infected bone defect models. Acta Biomater 2018;79:265–75.
[32] Tan H, Peng Z, Li Q, Xu X, Guo S, Tang T. The use of quaternised chitosan-loaded PMMA to inhibit biofilm formation and downregulate the virulence-associated gene expression of antibiotic-resistant staphylococcus. Biomaterials 2012;33(2):365–77.
[33] Lai Y, Li Y, Cao H, Long J, Wang X, Li L, et al. Osteogenic magnesium incorporated into PLGA/TCP porous scaffold by 3D printing for repairing challenging bone defect. Biomaterials 2019;197:207–19.
[34] Zhang Q, Oh JH, Park CH, Baek JH, Ryoo HM, Woo KM. Effects of dimethyloxalylglycine-embedded poly(ε-caprolactone) fiber meshes on wound healing in diabetic rats. ACS Appl Mater Interfaces 2017;9(9):7950–63.
[35] Chang M, Nguyen TT. Strategy for treatment of infected diabetic foot ulcers. Acc Chem Res 2021;54(5):1080–93.
[36] Ma R, Lai YX, Li L, Tan HL, Wang JL, Li Y, et al. Bacterial inhibition potential of 3D rapid-prototyped magnesium-based porous composite scaffolds–an in vitro efficacy study. Sci Rep 2015;5:13775.
[37] Robinson DA, Griffith RW, Shechtman D, Evans RB, Conzemius MG. In vitro antibacterial properties of magnesium metal against Escherichia coli, Pseudomonas aeruginosa and Staphylococcus aureus. Acta Biomater 2010;6(5):1869–77.